Electronic Structure Analysis of the Difference between Cs_2AgF_4 and Rb_2MnF_4 in Their Magnetic Properties and Single-Crystal Structure Determination of Rb_2MnF_4

D. Dai and M.-H. Whangbo*

Department of Chemistry, North Carolina State University, Raleigh, North Carolina 27695-8204

J. Köhler* and C. Hoch

Max-Planck-Institut für Festkörperforschung, Heisenbergstrasse-1, D-70569 Stuttgart, Germany

A. Villesuzanne

Institut de Chimie de la Matière Condensée de Bordeaux (ICMCB-CNRS), Université Bordeaux 1, 87 Avenue du Dr. A. Schweitzer, 33608 Pessac Cedex, France

Received February 24, 2006. Revised Manuscript Received May 12, 2006

The single-crystal structure of Rb_2MnF_4 was determined, and first principles electronic band structure calculations were carried out for Cs_2AgF_4 and Rb_2MnF_4. The intralayer spin exchange is calculated to be ferromagnetic in Cs_2AgF_4 but antiferromagnetic in Rb_2MnF_4, in agreement with experiments. Our analysis indicates that the ferromagnetism in Cs_2AgF_4 originates from the spin polarization of the doubly occupied $d_{x^2-y^2}$ band, which is induced by the $d_{z^2}-p-d_{x^2-y^2}$ orbital interactions through the Ag−F−Ag bridges, and similar interactions are not effective in La_2CuO_4. The crystal structure of Rb_2MnF_4 is quite similar to that of K_2MnF_4, as expected. However, most Rb_2MnF_4 crystals consist of numerous very thin platelets that are slightly skewed and/or shifted with respect to each other.

Introduction

The ternary layered fluorides A_2MnF_4 (A = K, Rb) have been studied as ideal two-dimensional (2-D) square-lattice Heisenberg antiferromagnets.[1−8] K_2MnF_4 has a K_2NiF_4-type structure,[9] and Rb_2MnF_4 is considered to be isostructural with K_2MnF_4, but its structure has not been reported. The ternary layered fluoride Cs_2AgF_4 crystallizes also in the K_2NiF_4-type structure, but it is a 2-D square-lattice Heisenberg ferromagnet.[10,11] Each MnF_4 layer of K_2MnF_4 is made up of corner-sharing MnF_6 octahedra containing high-spin Mn^{2+} (d^5) ions, and the MnF_6 octahedra are almost regular in shape with $Mn-F_{eq} = 2.087$ Å, $Mn-F_{ax} = 2.104$ Å, and linear $Mn-F_{eq}-Mn$ bridges (here, F_{eq} and F_{ax} refer to the equatorial and axial F atoms, respectively). In Cs_2AgF_4, the AgF_6 octahedra containing Ag^{2+} (d^9) ions are axially flattened with $Ag-F_{eq} = 2.291$ Å, $Ag-F_{ax} = 2.129$ Å, and linear $Ag-F_{eq}-Ag$ bridges. The fact that A_2MnF_4 (A = Rb, K) and Cs_2AgF_4 are both 2-D square-lattice Heisenberg magnets means that their spin exchange interactions between adjacent MF_4 (M = Mn, Ag) layers are negligible as compared with those within each MF_4 layer, and hence, the $Mn-F_{eq}-Mn$ superexchange is antiferromagnetic (AFM) in A_2MnF_4 ($J < 0$), but the $Ag-F_{eq}-Ag$ superexchange is ferromagnetic (FM) in Cs_2AgF_4 ($J > 0$).

It is an interesting question as to why the intralayer spin exchange is FM in Cs_2AgF_4 but AFM in Rb_2MnF_4. Cs_2AgF_4 is similar in crystal and electronic structures to La_2CuO_4, which is a precursor to high-T_C superconductors. Both have a K_2NiF_4-type structure and possess spin 1/2 divalent metal ions M^{2+} (d^9) (M = Ag, Cu). Nevertheless, they are quite different in magnetic properties; La_2CuO_4 is a 2-D antiferromagnet,[12] while Cs_2AgF_4 is a 2-D ferromagnet. Why these apparently similar compounds differ in their magnetic properties has not been explained. Ferromagnetism in materials can arise from a number of different mechanisms, which include Stoner,[13] double exchange,[14] spin exchange,[15] spin

(1) Birgeneau, R. J.; Guggenheim, H. J.; Shirane, G. *Phys. Rev. B* **1970**, *1*, 2211.
(2) Birgeneau, R. J.; Guggenheim, H. J.; Shirane, G. *Phys. Rev. B* **1973**, *8*, 304.
(3) de Wijn, H. W.; Walker, L. R.; Walstedt, R. E. *Phys. Rev. B* **1973**, *8*, 285.
(4) Cowley, R. A.; Shirane, G.; Birgeneau, R. J.; Guggenheim, H. G. *Phys. Rev. B* **1977**, *15*, 4292.
(5) Ikeda, H.; Tamura, T.; Nakashima, S. *J. Phys. C: Solid State Phys*. **1987**, *20*, L461.
(6) Iwasa, K.; Nishi, M.; Ikeda, H.; Suzuki, J. *J. Phys. Soc. Jpn*. **1994**, *63*, 1900.
(7) Leheny, R. L.; Christianson, R. J.; Birgeneau, R. J.; Erwin, R. W. *Phys. Rev. Lett*. **1999**, *82*, 418.
(8) Huberman, T.; Coldea, R.; Cowley, R. A.; Tennant, D. A.; Leheny, R. L.; Christianson, R. J.; Frost, C. D. *Phys. Rev. B* **2005**, *72*, 014413.
(9) Babel, D.; Herdtweck, E. *Z. Anorg. Allg. Chem*. **1982**, *487*, 75.
(10) Odenthal, R. H.; Paus, D.; Hoppe, R. *Z. Anorg. Allg. Chem*. **1974**, *407*, 144.
(11) McLain, S. E.; Tennant, D. A.; Turner, J. F. C.; Barnes, T.; Dolgos, M. R.; Proffen, T.; Sales, B. C.; Bewley, R. I.; http://xxx.lanl.gov/pdf/cond-mat/0509194.
(12) (a) Yang, B. X.; Mitsuda, S.; Shirane, G.; Yamaguchi, Y.; Yamauchi, H.; Syono, Y. *J. Phys. Soc. Jpn.* **1987**, *56*, 2283. (b) Vaknin, D.; Sinha, S. K.; Moncton, D. E.; Johnston, D. C.; Newsam, J. M.; Safinya, C. R.; King, H. E., Jr. *Phys. Rev. Lett.* **1987**, *58*, 2802.
(13) Stoner, E. C. *Proc. R. Soc. London, Ser. A* **1938**, *165*, 372.
(14) Zener, C. *Phys. Rev.* **1951**, *82*, 403.

10.1021/cm060465+ CCC: $33.50
Published on Web 06/14/2006

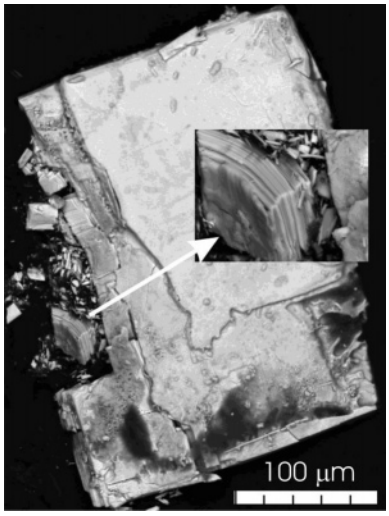

Figure 1. Scanning electron microscopy image of a piece of Rb_2MnF_4 indicating its layer-like structure. A piece was broken by slightly touching a thin crystal of Rb_2MnF_4 with the tip of a steel needle.

polarization,[16] metal−metal bonding,[17] and orbital ordering[18,19] mechanisms. Why ferromagnetism occurs in Cs_2AgF_4 is not well-understood, although orbital ordering has been suggested to be the origin.[11] In the present paper, we probe these questions on the basis of first principle electronic band structure calculations. Another objective of our work is to determine the crystal structure of Rb_2MnF_4, for which numerous studies of magnetic properties have been performed without knowing its crystal structure.

Synthesis and Single-Crystal Structure of Rb_2MnF_4

Starting materials RbF (Alfa, 99.9%) and MnF_2 (Alfa, 99.9%) were dried at 250 °C in a dynamic vacuum of 10^{-5} Torr. RbF and MnF_2 were mixed in a 2:1 molar ratio and ground in an argon-filled drybox, and the resulting mixture was pressed into a pellet. The pellet was placed into a platinum tube and subsequently sealed in an argon-filled quartz glass tube. The sealed ampule was heated to 820 °C with a heating rate of 5 °C/min, held for 16 h, and then cooled to room temperature with a rate of 2 °C/min to obtain a powder sample of Rb_2MnF_4. Since Rb_2MnF_4 melts incongruently, the powder sample contains a mixture of RbF, $RbMnF_3$, and Rb_2MnF_4, as verified by X-ray powder diffraction data (collected on a STOE STADI-P powder diffractometer equipped with a mini-PSD detector with a rotating sample in symmetric transmission mode, Ge monochromator, and Cu $K\alpha_1$ radiation). The powder X-ray refinement of the tetragonal unit cell of Rb_2MnF_4 resulted in $a = 4.322(1)$ Å and $c = 13.884(1)$ Å.

Colorless transparent single crystals of Rb_2MnF_4 with a plate-like habit were selected after physically fragmenting a sample under an optical microscope. However, the crystals are very brittle, and most of them consisted of numerous very thin platelets (Figure 1), which were slightly skewed and/or shifted with respect to each other due most likely to the mechanical stress. Thus, it was necessary to check their suitability for intensity data collection by recording photographs on a Stoe Image Plate IPDS diffractometer. Indeed, a more or less significant disorder was observed for all of the crystals, as shown for one example in Figure 2. A similar situation was found for crystals of K_2CuF_4, in which the stacking of the CuF_4 layers along the [001] direction is disordered.[20]

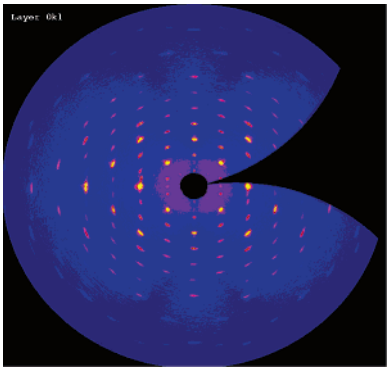

Figure 2. Photograph of the 0*kl* layer of a representative Rb_2MnF_4 crystal emulated from data collected with a Stoe IPDS diffractometer.

After exposing an as-prepared pellet of Rb_2MnF_4 with its byproducts (RbF and $RbMnF_3$) to air for 1 day, the sample becomes partly liquid due to hydrate formation of the moisture sensitive RbF. This makes it possible to easily separate crystals of Rb_2MnF_4 from the rest without any mechanical stress. One such crystal of Rb_2MnF_4 was found to have an acceptable quality for single-crystal X-ray diffraction measurements, which we performed using Ag Kα radiation with a graphite monochromator. The intensities were corrected for Lorentz and polarization effects, and a semiempirical absorption correction was applied on the basis of the ψ-scans. Table 1 summarizes the crystallographic data and experimental conditions of the data collection and refinement. The structure was refined against F^2 using the SHELX-97 program[21a] to residuals $wR_2 = 9.9\%$ and $R_1 = 6.5\%$ for all 88 independent reflections. The displacement factors of the atoms were taken into account in the anisotropic harmonic approximation. Atomic scattering factors and anomalous dispersion corrections were taken from ref 21b. The atomic position parameters and isotropic displacement factors for Rb_2MnF_4 are given in Table 2. The anisotropic displacement parameters for Rb_2MnF_4 are given in Table S1 of the Supporting Information.

As in K_2MnF_4, each MnF_6 octahedron in Rb_2MnF_4 is almost regular in shape with $Mn-F_{eq} = 2.116(1)$ Å, $Mn-F_{ax} = 2.091(2)$ Å, and linear $Mn-F_{eq}-Mn$ bridges. The Rb^+ ions are located in the centers of the squares of four adjacent F_{ax} atoms so that Rb_2MnF_4 slabs are formed (Figure 3). Each Rb^+ ion of one Rb_2MnF_4 slab is coordinated to one F_{ax}^- ion of its adjacent Rb_2MnF_4 slab with a distance of 2.802 Å. This weak interslab interaction is reflected by the petalled habit of most Rb_2MnF_4 crystals (Figure 2). The weak bonding between the slabs is also indicated by the significantly larger c/a ratio for Rb_2MnF_4 (3.28) as compared with that for K_2MnF_4 (3.18).

Intralayer Spin Exchange Interactions of Rb_2MnF_4 and Cs_2AgF_4

To probe the difference between Rb_2MnF_4 and Cs_2AgF_4 in their intralayer spin exchange interactions, we carried out density functional theory (DFT) spin polarized electronic band structure calculations using the full-potential augmented

(15) Goodenough, J. B. *Magnetism and the Chemical Bond*; Wiley: Cambridge, MA, 1963.
(16) Kahn, O. *Molecular Magnetism*; VCH: New York, 1993; Ch. 12.
(17) Villesuzanne, A.; Whangbo, M.-H. *Inorg. Chem.* **2005**, *44*, 6339.
(18) Kugel, K. I.; Khomskii, D. I. *Sov. Phys. Usp.* **1982**, *25*, 231.
(19) Koo, H.-J.; Whangbo, M.-H. *J. Solid State Chem.* **2000**, *151*, 96.
(20) Haegele, R.; Babel, D. *Z. Anorg. Allg. Chem.* **1974**, *409*, 11.
(21) (a) Sheldrick, G. M. *SHELXL-97, Program for the Refinement of Crystal Structures from Diffraction Data*; Universität Göttingen: Göttingen, Germany, 1997. (b) Hahn, T., Ed. *International Tables of Crystallography*, Vol. A, 4th ed.; Kluwer: Dordrecht, The Netherlands, 1995.

Table 1. Crystallographic Data and Parameters of Data Collection and Structure Refinements of Rb_2MnF_4 at Room Temperature[a]

space group; Z	$I4/mmm$ (No. 139); 2
unit cell dimensions[b] (Å)	$a = 4.232(1)$, $c = 13.885(3)$
$F(000)$	270
cryst size (mm^3)	$0.02 \times 0.5 \times 0.5$
μ (Ag Kα), λ (Ag Kα)	22.057 mm^{-1}, 0.56086 Å
measuring mode	$d = 60$ mm, oscillation, $0 \le \varphi \le 240.0°$, *step width 1.0°*
Θ-range for data collection (deg)	4.6−20
limiting indices	$-5 < h < 4$, $-5 < k < 4$, $-16 < l < 16$
reflns collected	487
ind reflns	88
R_{int} (%)	12.9
no. of free parameters, GOF	12, 1.359
R1, wR2 ($I > 2\sigma(I)$) (%)	6.5, 9.8
R1, wR2 (all data) (%)	6.5, 9.9
weighting (a, b)	0.000, 8.3306[c]

[a] Further details of the crystal structure determination may be found from the Fachinformationzentrum Energie, Physik, Mathematik, D-76344 Eggenstein-Leopoldshafen 2, on quoting the depository number CSD-416259, the names of the authors, and the journal citation. [b] Powder diffraction data. [c] Weighting scheme: $1/[\sigma^2(F_o^2) + (aP)^2 + bP]$ with $P = [\max(F_o^2,0) + 2F_c^2]/3$.

Table 2. Atomic Coordinates and Equivalent Isotropic Displacement Parameters (pm^2) for Rb_2MnF_4

atom	position	x/a	z/c	B (is/eq)
Rb	4*e*	0	0.3524(1)	0.0222(9)
Mn	2*a*	0	0	0.0163(12)
F(1)	4*e*	0.5	0	0.0240(30)
F(2)	4*c*	0	0.1506(9)	0.0210(30)

Table 3. Electronic Energy Difference Δ*E* (per Formula Unit) between AFM and FM States for Rb_2MnF_4 and Cs_2AgF_4 and Intralayer Nearest-Neighbor Spin Exchange Parameters *J*

	Δ*E* (meV)	J_{cal} (meV)	J_{exp} (meV)
Rb_2MnF_4	−14.8	−0.59	−0.654[a]
Cs_2AgF_4	+28.0	+28.0	+3.793[b]

[a] Reference 1. [b] Reference 11.

plane wave method implemented in the WIEN2k package[22,23] within the generalized gradient approximation of Perdew et al. for the exchange-correlation energy.[24] We employed the muffin-tin radii of 2.11 au for Mn, 2.12 au for Ag, 1.88 au for F, and 2.50 au for Rb and Cs. The plane wave cutoff was $R_{mt}K_{max} = 7$, and the irreducible wedge of the Brillouin zone was sampled with a 100 *k*-point mesh. For both Rb_2MnF_4 and Cs_2AgF_4, we examined two ordered spin arrangements (i.e., the FM and AFM arrangements depicted in Figure 4).

The electronic energy difference (per formula unit) between the AFM and the FM states, $\Delta E = E_{AFM} - E_{FM}$, calculated for Rb_2MnF_4 and Cs_2AgF_4 is listed in Table 3. Our calculations predict that the AFM state is more stable than the FM state for Rb_2MnF_4, while the opposite is the case for Cs_2AgF_4, in agreement with experiments. As already mentioned, the energy difference between the AFM and the FM states of A_2MF_4 is primarily determined by the intralayer $M-F_{eq}-M$ (M = Mn, Ag) superexchange interactions *J*. Suppose that a spin dimer is made up of two equivalent spin sites containing *N* unpaired spins each, and the spin exchange interaction between them is described by the spin exchange parameter *J*. Then, the energies of the FM and AFM states (i.e., the highest-spin and broken-symmetry states, respectively) of the spin dimer are given by $-N^2J/4$ and $N^2J/4$,

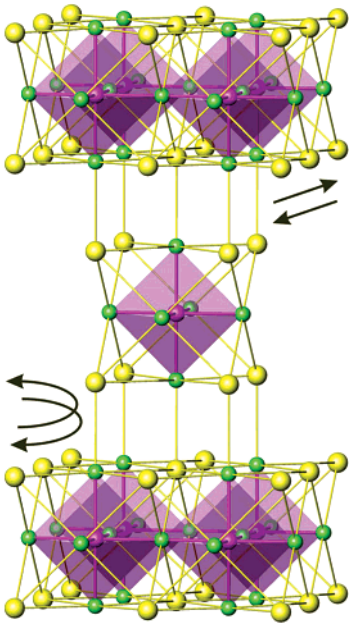

Figure 3. Perspective view of the crystal structure of Rb_2MnF_4. The pink circles represent the Mn atoms, the yellow circles the Rb atoms, and the green circles the F atoms. Each MnF_6 octahedron is indicated by shading. The arrows indicate possible shift or twisting of adjacent Rb_2MnF_4 slabs.

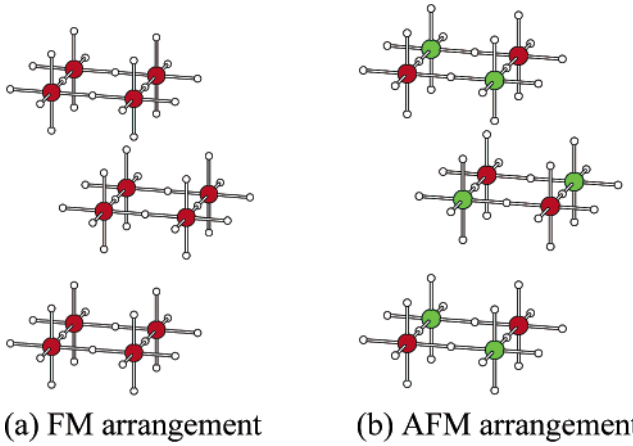

Figure 4. (a) FM and (b) AFM arrangements of spins in Rb_2MnF_4 and Cs_2AgF_4.

(22) Blaha, P.; Schwarz, K.; Madsen, G.; Kvasnicka, D.; Luitz, J. *WIEN2k, An Augmented Plane Wave + Local Orbitals Program for Calculating Crystal Properties*; Technical Universität Wien: 2001. See also: http://www.wien2k.at/.
(23) (a) Sjöstedt, E.; Nordström, L.; Singh, D. *Solid State Commun.* **2000**, *114*, 15. (b) Madsen, G. K. H.; Blaha, P.; Schwarz, K.; Sjöstedt, E.; Nordström, L. *Phys. Rev. B* **2001**, *64*, 195134.
(24) Perdew, J. P.; Burke, S.; Ernzerhof, M. *Phys. Rev. Lett.* **1996**, *77*, 3865.

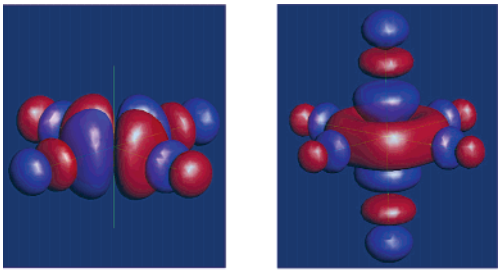

Figure 5. (a) $d_{x^2-y^2}$ and (b) d_{z^2} orbitals of an isolated AgF_6 octahedron taken from the crystal structure of Cs_2AgF_4.

respectively.[25] Thus, for a 2-D square-lattice described by the spin Hamiltonian defined by the nearest-neighbor spin exchange parameter J, the energy of the FM state is $-N^2J/2$ per spin site (i.e., $(1/2)4 \times (-N^2J/4)$) and that of the AFM state by $N^2J/2$ per spin site (i.e., $(1/2)4 \times (N^2J/4)$). Consequently, in terms of this spin Hamiltonian, the energy difference between the AFM and the FM states is given by N^2J. Then, the spin change parameter J is related to the electronic energy difference ΔE between the AFM and the FM states by[25−28]

$$J = \Delta E/N^2 \tag{1}$$

where $N = 5$ for the high-spin Mn^{2+} ions of Rb_2MnF_4, and $N = 1$ for the Ag^{2+} ions of Cs_2AgF_4. The spin exchange parameters of Rb_2MnF_4 and Cs_2AgF_4 thus calculated (J_{cal}) are compared with the corresponding experimental values (J_{exp}) in Table 3. For Rb_2MnF_4, the calculated spin exchange parameter is in good agreement with experiment. For Cs_2AgF_4, the calculation overestimates the spin exchange parameter by a factor of approximately seven. In general, DFT electronic structure calculations are known to overestimate the magnitude of spin exchange interactions.[25−28]

Origin of the Ferromagnetism in Cs_2AgF_4

As a possible cause for the ferromagnetism in the AgF_4 layers of Cs_2AgF_4, orbital ordering has been suggested.[11] Orbital ordering is a phenomenon associated with incompletely filled degenerate levels.[18,19] Each AgF_6 octahedron of Cs_2AgF_4 is axially flattened, although slightly, so that its e_g-block levels (i.e., the $d_{x^2-y^2}$ and d_{z^2} levels) cannot be degenerate. This distortion makes the $d_{x^2-y^2}$ level lie lower than the d_{z^2} level (Figure 5) (by approximately 0.37 eV according to our extended Hückel tight binding calculations[29] using the atomic orbital parameters given in Table S2 of the Supporting Information), thereby leading to the electron configuration $(\cdots)^2(d_{x^2-y^2})^2(d_{z^2})^1$, where $(\cdots)^2$ means that all the levels lying below the $d_{x^2-y^2}$ level are each doubly occupied. Furthermore, our electronic band structure calculations, which do not include orbital ordering, predict the FM state to be more stable than the AFM state. Thus, orbital ordering cannot be responsible for the ferromagnetism of Cs_2AgF_4.

The total density of states (TDOS) and the partial density of states (PDOS) calculated for the FM and AFM states of Cs_2AgF_4 are presented in Figure 6. In the AFM state, the up-spin/down-spin $d_{x^2-y^2}$ bands lie lower than the up-spin/down-spin d_{z^2} bands, and are completely filled, while the down-spin d_{z^2} band is largely empty (Figure 6a). This is the feature expected from the nonspin polarized view that the singly occupied d_{z^2} orbital lies above the doubly occupied $d_{x^2-y^2}$ orbital in each AgF_6 octahedron. In the FM state, the up-spin/down-spin $d_{x^2-y^2}$ bands overlap with the up-spin/down-spin d_{z^2} bands such that the down-spin $d_{x^2-y^2}$ band is partially empty, and the down-spin d_{z^2} band is partially occupied (Figure 6b). In the following, we discuss the reason for the difference between the AFM and the FM states and its implication concerning the ferromagnetism in Cs_2AgF_4.

In DFT, magnetic states are described by spin polarized electronic structures, in which up-spin/down-spin bands of a given orbital type possess different orbital compositions and different energy levels. In understanding the spin polarized electronic structures of Cs_2AgF_4, it is important to estimate the ordering of the up-spin/down-spin d-block levels of an AgF_6 octahedron, in particular, the up-spin/down-spin $d_{x^2-y^2}$ levels and the up-spin/down-spin d_{z^2} levels. Let us denote the d_{z^2} and $d_{x^2-y^2}$ levels in the absence of electron−electron repulsion as e_2^0 and e_1^0, respectively. Then, from the electron configuration $(\cdots)^2(d_{x^2-y^2})^2(d_{z^2})^1$, the up-spin and down-spin $d_{z^2}/d_{x^2-y^2}$ levels in the presence of electron−electron repulsion are expressed as[17,30−33]

$$\begin{aligned} e_2{\downarrow} &\approx e_2^0 + U + 2U' - K \\ e_2{\uparrow} &\approx e_2^0 + 2U' - K \\ e_1{\downarrow} &\approx e_1^0 + U \\ e_1{\uparrow} &\approx e_1^0 + U - K \end{aligned} \tag{2}$$

where U is the on-site Coulomb repulsion for two electrons in a same metal d orbital, U' is that for two electrons in two different metal d orbitals, and K is the exchange repulsion between two electrons of an identical spin in two different d orbitals. In general, $U > U' > K$. According to eq 2, therefore, the relative ordering of these levels is given by

$$e_1{\uparrow} < e_1{\downarrow} < e_2{\uparrow} < e_2{\downarrow} \tag{3}$$

When the 4d orbitals of nearest-neighbor Ag^{2+} ions interact through the orbitals of the bridging F^- ions in all the Ag−F_{eq}−Ag bridges, the above levels become bands. The ordering of the up-spin/down-spin $d_{x^2-y^2}$ and d_{z^2} bands in the FM state is in good agreement with that predicted by eq 3.

(25) Dai, D.; Whangbo, M.-H. *J. Chem. Phys.* **2001**, *114*, 2887.
(26) Dai, D.; Koo, H.-J.; Whangbo, M.-H. *J. Solid State Chem.* **2003**, *175*, 341.
(27) Grau-Crespo, R.; de Leeuw, N. H.; Catlow, C. R. *J. Mater. Chem.* **2003**, *13*, 2848.
(28) Dai, D.; Whangbo, M.-H.;Koo, H.-J.; Rocquefelte, X.; Jobic, S.; Villesuzanne, A. *Inorg. Chem.* **2005**, *44*, 2407.
(29) Our calculations were carried out by employing the SAMOA (Structure and Molecular Orbital Analyzer) program package (Dai, D.; Ren, J.; Liang, W.; Whangbo, M.-H.; http://chvamw.chem.ncsu.edu/, 2002).
(30) Brandow, B. H. *Adv. Phys.* **1977**, *26*, 651.
(31) Whangbo, M.-H. *Inorg. Chem.* **1980**, *19*, 1728.
(32) Pouchard, M.; Villesuzanne, A.; Doumerc, J.-P. *J. Solid State Chem.* **2001**, *162*, 282.
(33) Whangbo, M.-H.; Koo, H.-J.; Villesuzanne, A.; Pouchard, M. *Inorg. Chem.* **2002**, *41*, 1920.

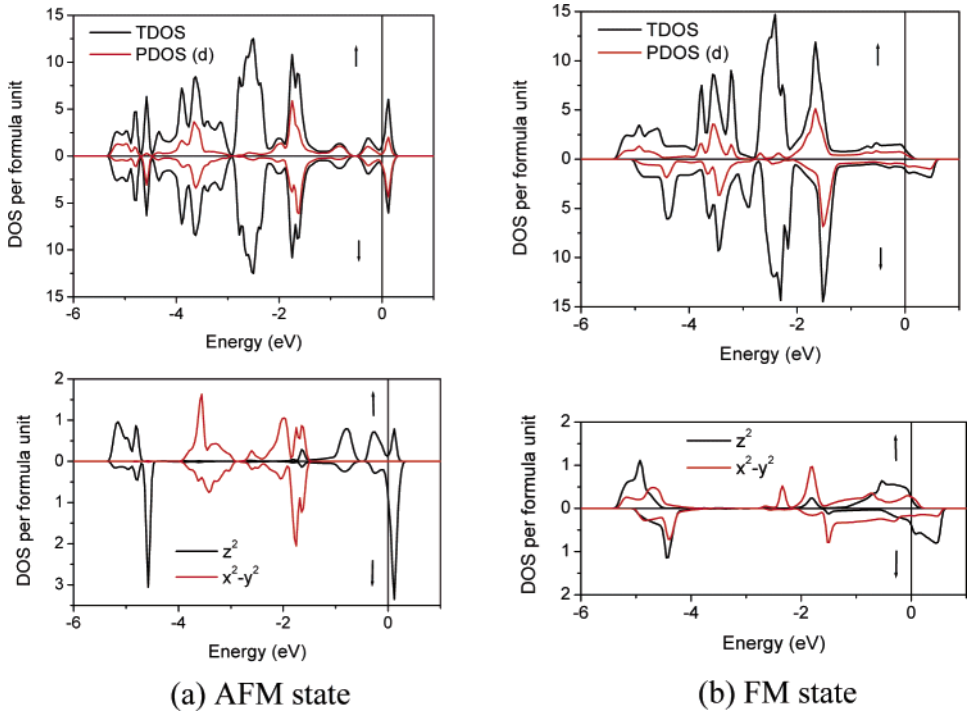

Figure 6. TDOS and PDOS plots calculated for the (a) AFM and (b) FM states of Cs_2AgF_4.

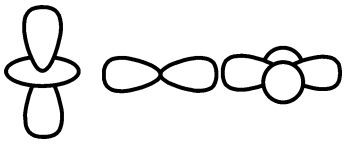

Figure 7. $d_{z^2}-p-d_{x^2-y^2}$ orbital interaction that can take place in the $Ag-F_{eq}-Ag$ bridges of Cs_2AgF_4 and in the $Cu-O_{eq}-Cu$ bridges of La_2CuO_4.

In the FM state, the up-spin/down-spin $d_{x^2-y^2}$ bands overlap with the up-spin/down-spin d_{z^2} bands (Figure 6b) because the following two conditions are satisfied: (1) in each $Ag-Feq-Ag$ bridge, the $4d_{z^2}$ orbital of one Ag^{2+} ion can interact with the $4d_{x^2-y^2}$ orbital of the other Ag^{2+} ion through the $2p_x$ or $2p_y$ orbital of the bridging F^- ion (Figure 7). (2) In the FM state, the orbitals of nearest-neighbor Ag^{2+} ions are allowed to interact through the $Ag-F_{eq}-Ag$ bridge because the two ions have the same spin (Figure 4a). In the AFM state, however, the condition (2) is not satisfied because the nearest-neighbor Ag^{2+} ions have different spins (Figure 4b). In the AFM state, therefore, each $Ag-F_{eq}-Ag$ bridge does not allow the $4d_{z^2}$ orbital of one Ag^{2+} ion to interact with the $4d_{x^2-y^2}$ orbital of the other Ag^{2+} ion through the $2p_x$ or $2p_y$ orbital of the bridging F^- ion. As a consequence, the up-spin/down-spin $d_{x^2-y^2}$ bands become narrow and do not overlap with the up-spin/down-spin d_{z^2} bands.

Why the FM state is energetically favored over the AFM state can be accounted for in part on the basis of on-site repulsion. Suppose that the up-spin and down-spin populations of a given d orbital at each Ag^{2+} site are $n_\uparrow$ and $n_\downarrow$, respectively. Then, the total on-site repulsion associated with that d orbital population is given by $n_\uparrow n_\downarrow U$.[34] If $n_\uparrow + n_\downarrow =$ constant, this repulsion is maximum when $n_\uparrow = n_\downarrow$. In the AFM state, $n_\uparrow = n_\downarrow = 1$ for the $4d_{x^2-y^2}$ orbital because the up-spin and down-spin $d_{x^2-y^2}$ bands are fully occupied (Figure 6a). In the FM state, $n\uparrow = 1$ and $n\downarrow < 1$ for the $4d_{x^2-y^2}$ orbital because the up-spin $d_{x^2-y^2}$ band is completely filled, while the down-spin $d_{x^2-y^2}$ band is partially empty (Figure 6b). Consequently, the repulsion $n\uparrow n\downarrow U$ associated with the $4d_{x^2-y^2}$ orbital occupation is less in the FM state than in the AFM state. In the FM state, the partial occupation of the down-spin d_{z^2} band will bring about some additional repulsion between the $d_{x^2-y^2}$ and the d_{z^2} orbitals. However, this effect would be less than the energy lowering from the reduction of the on-site repulsion associated with the $4d_{x^2-y^2}$ orbital since $U' < U$. Another factor favoring the FM state over the AFM state is that in the FM state, the F 2p levels in each $Ag-F_{eq}-Ag$ bridge can be strongly stabilized by in-phase combination with the $4d_{x^2-y^2}$ orbitals of Ag, as can be seen by comparing the PDOS plots of the $d_{x^2-y^2}$ orbitals in Figure 6a,b; the lower energy part of the PDOS plots occurs below -4 eV in the FM state but above -4 eV in the AFM state.

Discussion

In essence, the ferromagnetism in Cs_2AgF_4 is caused by the spin polarization of the $d_{x^2-y^2}$ bands, which is induced by the $d_{z^2}-p-d_{x^2-y^2}$ orbital interactions through the $Ag-F_{eq}-Ag$ bridges (Figure 7). The extended nature of the Ag 4d orbital is favorable for the overlap between the d and the p orbitals of each $Ag-F_{eq}$ bond, and the weak distortion of each AgF_6 octahedron makes the $d_{x^2-y^2}$ level only slightly lower than the d_{z^2} level. These two factors strengthen the $d_{z^2}-p-d_{x^2-y^2}$ orbital interactions through the $Ag-F_{eq}-Ag$ bridges in Cs_2AgF_4. The corresponding $d_{z^2}-p-d_{x^2-y^2}$ interactions in La_2CuO_4 (through the $Cu-O_{eq}-Cu$ bridges) should be considerably weaker because the Cu 3d orbital is more contracted and because the distortion of each CuO_6 octahedron is strong (with $Cu-O_{eq} = 1.90$ Å and $Cu-O_{ax} = 2.40$

(34) Whangbo, M.-H. *J. Chem. Phys.* **1980**, *73*, 3854.

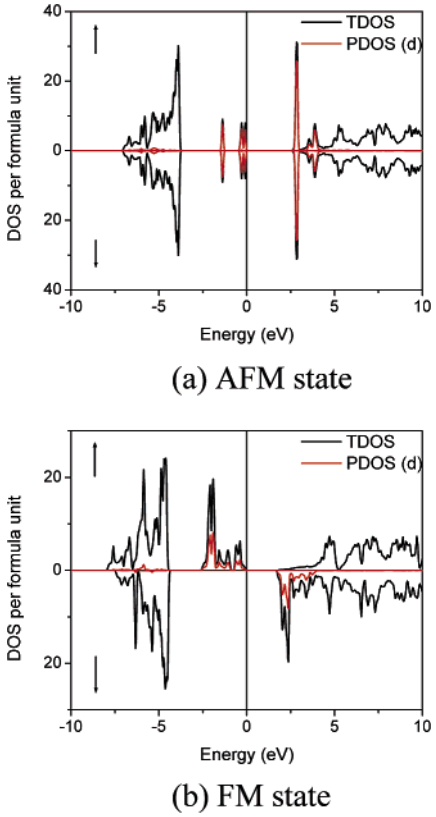

Figure 8. TDOS and PDOS plots calculated for the (a) AFM and (b) FM states of Rb_2MnF_4.

Å)[35] so that the d_{z^2} level lies considerably lower than the $d_{x^2-y^2}$ level (by approximately 1.3 eV according to our extended Hückel tight binding calculations[29] using the atomic orbital parameters in Table S2 of the Supporting Information). Consequently, in La_2CuO_4, the intralayer spin exchange is dominated by the $d_{x^2-y^2}-p-d_{x^2-y^2}$ orbital interactions of the $Cu-O_{eq}-Cu$ bridges, which leads to strong antiferromagnetism.[12,19]

Rb_2MnF_4 contains high-spin $Mn^{2+}(d^5)$ ions and hence does not have any doubly filled d-block band (Figure 8). Thus, the spin polarization mechanism leading to ferromagnetism in Cs_2AgF_4 is not applicable to Rb_2MnF_4. Therefore, the magnetism of Rb_2MnF_4 is governed by the spin exchange[15] through the $Mn-F_{eq}-Mn$ bridges, which gives rise to antiferromagnetism. Note from Figure 8 that the d-block bands are wider in the FM state than in the AFM state. As already pointed out, this is so because the orbitals of nearest-neighbor Mn^{2+} ions are allowed to interact through the $Mn-F_{eq}-Mn$ bridge in the FM state, while this is not possible in the AFM state.

Conclusion

Our electronic structure calculations for Cs_2AgF_4 and Rb_2MnF_4 reproduce the experimental observation that the intralayer spin exchange is FM in Cs_2AgF_4 but AFM in Rb_2MnF_4. Analysis of the electronic structures calculated for the FM and AFM states of Cs_2AgF_4 indicates that the ferromagnetism in Cs_2AgF_4 originates from the spin polarization of the doubly occupied $d_{x^2-y^2}$ band, which is induced by the $d_{z^2}-p-d_{x^2-y^2}$ orbital interactions through the $Ag-F_{eq}-Ag$ bridges. These interactions are favorable in Cs_2AgF_4 because of the extended nature of the Ag 4d orbital and the weak distortion of each AgF_6 octahedron. Similar interactions are not favorable in La_2CuO_4 due to the contracted nature of the Cu 3d orbital and the strong distortion of each CuO_6 octahedron. The spin polarization mechanism found for Cs_2AgF_4 does not occur in Rb_2MnF_4 because Rb_2MnF_4 does not have any doubly filled d-block band.

As expected, the crystal structure of Rb_2MnF_4 is quite similar to that of K_2MnF_4. Nevertheless, our work shows that most Rb_2MnF_4 crystals consist of numerous very thin platelets that exhibit a slightly but significant disordered stacking along the *c*-axis. This would complicate the interpretation of the magnetic ordering in Rb_2MnF_4 along the *c*-direction.

Acknowledgment. The work at NCSU was supported by the Office of Basic Energy Sciences, Division of Materials Sciences, U.S. Department of Energy, under Grant DE-FG02-86ER45259.

Supporting Information Available: Table S1 of the anisotropic displacement parameters of Rb_2MnF_4 and Table S2 of the atomic orbital parameters employed for extended Hückel tight-binding calculations. This material is available free of charge via the Internet at http://pubs.acs.org.

CM060465+

(35) Longo, L. M.; Raccah, P. M. *J. Solid State Chem.* **1973**, *6*, 526.